Monthly Notices
of the
ROYAL ASTRONOMICAL SOCIETY

MNRAS **465,** 492–500 (2017)
Advance Access publication 2016 November 2

doi:10.1093/mnras/stw2798

Evidence for vacuum birefringence from the first optical-polarimetry measurement of the isolated neutron star RX J1856.5−3754

R. P. Mignani,[1,2★] V. Testa,[3★] D. González Caniulef,[4★] R. Taverna,[5] R. Turolla,[4,5] S. Zane[4] and K. Wu[4]

[1]*INAF – Istituto di Astrofisica Spaziale e Fisica Cosmica Milano, via E. Bassini 15, I-20133 Milano, Italy*
[2]*Janusz Gil Institute of Astronomy, University of Zielona Góra, Lubuska 2, PL-65-265 Zielona Góra, Poland*
[3]*INAF – Osservatorio Astronomico di Roma, via Frascati 33, I-00040 Monteporzio, Italy*
[4]*Mullard Space Science Laboratory, University College London, Holmbury St Mary, Dorking RH5 6NT, Surrey, UK*
[5]*Dipartimento di Fisica e Astronomia, Universitá di Padova, via Marzolo 8, I-35131 Padova, Italy*

Accepted 2016 October 25. Received 2016 October 25; in original form 2016 September 13

ABSTRACT

The 'Magnificent Seven' (M7) are a group of radio-quiet isolated neutron stars discovered in the soft X-rays through their purely thermal surface emission. Owing to the large inferred magnetic fields ($B \approx 10^{13}$ G), radiation from these sources is expected to be substantially polarized, independently of the mechanism actually responsible for the thermal emission. A large observed polarization degree (PD) is, however, expected only if quantum-electrodynamic (QED) polarization effects are present in the magnetized vacuum around the star. The detection of a strong linearly polarized signal would therefore provide the first observational evidence of QED effects in the strong-field regime. While polarization measurements in the soft X-rays are not feasible yet, optical polarization measurements are within reach also for quite faint targets, like the M7 which have optical counterparts with magnitudes ≈26–28. Here, we report on the measurement of optical linear polarization for the prototype, and brightest member, of the class, RX J1856.5−3754 ($V \sim 25.5$), the first ever for one of the M7, obtained with the Very Large Telescope. We measured a PD = 16.43 ± 5.26 per cent and a polarization position angle PA = 145.°39 ± 9.°44, computed east of the North Celestial Meridian. The PD that we derive is large enough to support the presence of vacuum birefringence, as predicted by QED.

Key words: techniques: polarimetric – stars: neutron – pulsars: individual: RX J1856.5 −3754.

1 INTRODUCTION

A class of seven radio-quiet isolated neutron stars (INSs), a.k.a. the 'Magnificent Seven' (M7), attracted the interest from the neutron star community soon after their discovery by *ROSAT* in the 1990s (see e.g. Turolla 2009, for a review). Owing to the purely thermal X-ray emission from the star surface ($kT \sim 50$–100 eV), unmarred by magnetospheric contributions, the M7 have always been considered unique laboratories to study the neutron star cooling process and hold the promise to provide a measurement of the star radius, which directly bears to the equation of state of matter at supranuclear density. The M7 exhibit slow X-ray pulsations ($P \sim 3$–11 s), likely produced by an inhomogeneous surface temperature distribution, and relatively large period derivatives ($\dot{P} \sim 10^{-14}$–10^{-13} s s^{-1}), from which ages of a few Myr and dipolar surface magnetic fields $B \sim 10^{13}$–10^{14} G were inferred. Evidence for such strong magnetic fields also came from the discovery of broad (EW ∼ 10–100 eV) absorption features at a few hundred eV superimposed to the thermal continuum, when interpreted as proton cyclotron and/or bound–free, bound–bound transitions in low-Z atoms. The nearly perfect blackbody (BB) spectrum of the M7 has been a puzzle throughout. Cooling INSs are expected to be covered by an atmosphere, which, however, does not emit a purely BB spectrum (see e.g. Potekhin 2014). An alternative possibility is that the outermost star layers are in a condensed form owing to the large magnetic field and relatively low temperature, giving rise to a so called 'bare' INS (Turolla, Zane & Drake 2004). Spectra from bare INSs would be close to a BB, although with some deviations.

Given the quite strong surface magnetic field of the M7, thermal radiation is expected to be polarized, either if emission is from a bare surface or from an atmosphere (see Turolla et al. 2004; Potekhin 2014). The polarization properties are quite different in

★ E-mail: rm2@mssl.ucl.ac.uk (RPM); vincenzo.testa@oa-roma.inaf.it (VT); denis.caniulef.14@ucl.ac.uk (DGC)

the two cases, although there are still uncertainties, especially at optical/ultraviolet (UV) wavelengths. One of the first predictions of quantum electrodynamics (QED), even before it was properly formulated, was vacuum birefringence, and, in particular, that a strong magnetic field affects the propagation of light through it (Heisenberg & Euler 1936; Weisskopf 1936). In thermally emitting INSs, radiation comes from a region comparable with the entire star surface, over which the magnetic field direction changes substantially. In the absence of QED vacuum polarization effects, this would produce a drastic depolarization of the radiation collected at infinity (Heyl, Shaviv & Lloyd 2003, see also Taverna et al. 2015; González Caniulef et al. 2016 and references therein). Vacuum birefringence dramatically increases the linear polarization of the observed radiation, from a level of a few per cent up to even ∼100 per cent, depending on the viewing geometry and the surface emission mechanism (Heyl & Shaviv 2000, 2002; Heyl et al. 2003; Taverna et al. 2015; González Caniulef et al. 2016). Detecting polarization in the thermal emission from the surface of an INS will be therefore extremely valuable. First, and independently on the physical conditions of the emitting region, the detection of a large degree of linear polarization in the signal would constitute the observational evidence of QED vacuum polarization effects in the strong-field regime. Secondly, the polarization observables can be compared with emission models and help to uncover the physical conditions of INS surfaces and atmospheres, ideally complementing spectral observations (Taverna et al. 2014; González Caniulef et al. 2016).

With X-ray polarimetry still moving its first steps and dedicated polarimetric missions, such as *XIPE*[1] (Soffitta et al. 2013) and *IXPE* (Weisskopf et al. 2013), having just been proposed, other energy ranges must be explored. Besides the X-rays, all M7 have been detected in the optical/near-UV (Kaplan et al. 2011), where well-tested techniques, even for objects as faint as INSs, can be exploited, as shown by the polarization measurements in rotation-powered pulsars (RPPs), for which we refer to Mignani et al. (2015) for an exhaustive summary. Whether the optical/near-UV emission is thermal and arises from the cooling surface is not entirely clear yet. However, in a few sources, notably including the prototype of the class, RX J1856.5−3754 (Walter & Matthews 1997), the low-energy spectral energy distribution follows quite closely a Rayleigh–Jeans distribution (Van Kerkwijk & Kulkarni 2001a). This is a robust indication that optical/near-UV photons are thermal and come from the surface, possibly from a cooler, larger region than that emitting the X-rays (as also supported by *XMM–Newton* data; Sartore et al. 2012).

Owing to their faintness, no optical polarimetric observations have been attempted so far for any of the M7. In this respect, the most promising target is RX J1856.5−3754. The source is the brightest ($V \sim 25.5$; Walter & Matthews 1997) and youngest (0.42 Myr; Mignani et al. 2013) among the M7. Its close distance (123^{+11}_{-15} pc; Walter et al. 2010), which minimizes the effects of foreground polarization, also concurs to make RX J1856.5−3754 the best target. Here, we present the results of phase-averaged linear polarization observations of RX J1856.5−3754, the first ever performed for one of the M7. We have carried out the observations with the Very Large Telescope (VLT) at the ESO Cerro Paranal Observatory (Chile). Observations and data analysis are described in Section 2, and results are presented in Section 3 and discussed in Section 4. Conclusions follow.

[1] http://www.isdc.unige.ch/xipe

2 OBSERVATIONS AND DATA REDUCTION

2.1 Observation description

We measured the optical linear polarization of RX J1856.5−3754 using the second Focal Reducer and low dispersion Spectrograph (FORS2; Appenzeller et al. 1998), mounted at the VLT Antu telescope. FORS2 features a red-sensitive mosaic MIT detector (two 4k × 2k CCDs aligned along the *X*-axis) and is equipped with polarization optics to measure either linear or circular time-averaged polarization. The polarization optics consists of a Wollaston prism as a beam-splitting analyser and two superachromatic phase retarder 3 × 3 plate mosaics (Boffin 2014). These retarder plates are installed on rotatable mountings to be moved in and out of the light path. In the imaging polarimetry mode (IPOL), a strip mask is produced in the FORS2 focal plane to separate the extraordinary and ordinary beams of polarized light as this passes through the retarder plate. The strip is formed by lacing every second multi-object spectrograph (MOS) slit jaw carrier arm across the instrument field of view. In this way, by taking two frames displaced by 22 arcsec in the *Y* direction, images corresponding to the extraordinary and ordinary beams are recorded on two adjacent MOS slitlets.

We used the four standard IPOL half-wave retarder-plate angles of 0°, 22.°5, 45°, and 67.°5, which correspond to the retarder-plate orientation relative to the Wollaston prism and are usually set with an accuracy better than 0.°1.[2] Both the axis of the detector optics and the zero-point of the half-wave retarder-plate angle are set such that the polarization position angle (PA) is measured eastwards from the North Celestial Meridian.

The observations of RX J1856.5−3754 were executed in service mode in 2015 May and June. We used the FORS2 low gain, normal readout (200 Kpix s^{-1}), standard-resolution mode (0.25 arcsec $pixel^{-1}$; 2 × 2 binning), and the high-efficiency v_{HIGH} filter ($\lambda = 555.0$ nm, $\Delta\lambda = 61.6$ nm). In order to cope with the variable sky polarization background, each observation block (OB) incorporated exposures (∼ 720 s) for each of the four retarder-plate angles. A total of 11 OBs were executed, for a total exposure of 7920 s per angle. Observations were performed in dark time, with average seeing of 0.84 arcsec, airmass below 1.1, and clear sky conditions.

2.2 Data reduction

A number of short exposures (<3 s) of polarized standard stars (Mathewson & Ford 1971; Whittet et al. 1992) were acquired for calibration purposes, as part of the FORS2 calibration plan. Observations of unpolarized standard stars were also acquired to monitor the FORS2 instrumental polarization at the aim position on the detector. We applied the same reduction procedure (bias-subtraction and flat-fielding) for both RX J1856.5−3754 and the standard stars using standard routines in IRAF.[3] Twilight flat-field images with no retarder plate along the light path were acquired on the same nights as the science images. For each OB, we finally obtained four reduced images, one for each of the four retarder-plate angles. We computed the FORS2 astrometry from the short-exposure (60 s) science acquisition image using stars from the Guide Star Catalogue 2 (GSC-2; Lasker et al. 2008) as a reference. After accounting for all

[2] www.eso.org/sci/facilities/paranal/instruments/fors.html

[3] IRAF is distributed by the National Optical Astronomy Observatories, which are operated by the Association of Universities for Research in Astronomy, Inc., under cooperative agreement with the National Science Foundation.

uncertainties (star centroids, GSC-2 absolute coordinate accuracy, etc.) our astrometric solution turned out to be accurate to better than 0.1 arcsec rms. We updated the RX J1856.5−3754 position at the epoch of our FORS2 observations (2015.37) by correcting for its proper motion μ using its reference coordinates (epoch 1999.7) measured with the *Hubble Space Telescope* (Kaplan, van Kerkwijk & Anderson 2002). The position uncertainty associated with the propagation of the proper motion errors (± 1 mas yr^{-1}) is negligible. The RX J1856.5−3754 coordinates at the epoch of our VLT observations are then $\alpha = 18^{\rm h}56^{\rm m}36\overset{\rm s}{.}03$; $\delta = -37^{\circ}54'37\overset{''}{.}11$ (J2000), and we used them as a reference to identify it in our VLT images.

2.3 Polarization measurement

Following the FORS2 manual (Boffin 2014), the degree of linear polarization of a source is calculated from the normalized Stokes parameters $P_{\rm U} \equiv U/I$ and $P_{\rm Q} \equiv Q/I$:

$$P_{\rm Q} = \frac{1}{2}\left\{\left(\frac{f^{\rm o}-f^{\rm e}}{f^{\rm o}+f^{\rm e}}\right)_{\alpha=0^{\circ}} - \left(\frac{f^{\rm o}-f^{\rm e}}{f^{\rm o}+f^{\rm e}}\right)_{\alpha=45^{\circ}}\right\} \quad (1)$$

$$P_{\rm U} = \frac{1}{2}\left\{\left(\frac{f^{\rm o}-f^{\rm e}}{f^{\rm o}+f^{\rm e}}\right)_{\alpha=22.5^{\circ}} - \left(\frac{f^{\rm o}-f^{\rm e}}{f^{\rm o}+f^{\rm e}}\right)_{\alpha=67.5^{\circ}}\right\}, \quad (2)$$

where $f^{\rm o}$ and $f^{\rm e}$ are the source fluxes in the ordinary (o) and extraordinary (e) beams, respectively, for each of the four retarder-plate angles α (0°, 22°.5, 45°, and 67°.5). The linear polarization degree (PD) and PA are, then, determined from $P_{\rm U}$ and $P_{\rm Q}$ as follows:

$$\mathrm{PD} = \sqrt{{P_{\rm Q}}^2 + {P_{\rm U}}^2} \quad (3)$$

$$\mathrm{PA} = \frac{1}{2}\arctan\left(\frac{P_{\rm U}}{P_{\rm Q}}\right). \quad (4)$$

By convention, in the following, we report the value of PD in per cent rather than in unity fractions. We note that for IPOL observations in the *V* band, the zero angle of the half-wave retarder plate is offset from 0° by 1°.8 (Boffin 2014) and this term must be subtracted from the PA defined in equation (4).

In order to increase the signal-to-noise ratio, we co-added all the reduced science images of RX J1856.5−3754 taken with the same retarder-plate angle (0°, 22°.5, 45°, and 67°.5) and used them to compute $f^{\rm o}$ and $f^{\rm e}$, hence the linear PD. For each angle, we aligned the single images using the IRAF tasks `ccdmap` and `ccdtrans`, with an average accuracy of a few hundredths of a pixel. We then applied the image co-addition with the IRAF routine `combine` and filtered cosmic ray hits using an average σ clipping. Fig. 1 shows a section of the image obtained from the co-addition of all exposures taken with all retarder-plate angles, zoomed on the RX J1856.5−3754 position.

To obtain a more robust detection of our target and improve on the photometry, we adopted a technique regularly used for studies of crowded stellar fields. First of all, we carefully aligned and registered all the images, regardless of the retarder-plate angle, and co-added them to create a master image, which we used as a reference for the source detection in each of the co-added 0°, 22°.5, 45°, 67°.5 retarder-plate angle images. This method, is well-suited to detect faint objects and improve the precision on the object centroid determination. As a subsequent step, we used the task *daofind* in the IRAF package DAOPHOT (Stetson 1987, 1994), which we ran on the master image to obtain a master source list that we used as a reference for the object detection in each of the four images above by keeping the objects' centroids fixed. In this way, we minimize the degrees of freedom in the photometry fit and ensure a better flux measurement for fainter objects, decreasing the photometry error by ∼20 per cent. From the master source list we also selected a number of stars to compute the model point spread function (PSF) for each of the four co-added images above by fitting the intensity profiles of a number of suitable stars in the field of view.

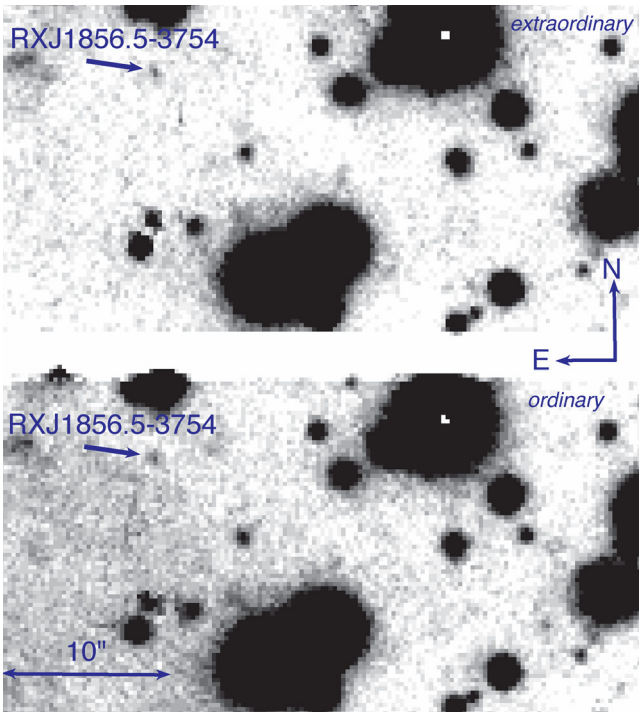

Figure 1. Section of the FORS2 IPOL $v_{\rm HIGH}$-band image of the RX J1856.5−3754 field obtained from the co-addition of all exposures taken with all retarder-plate angles. The optical counterpart to RX J1856.5−3754 is marked by the arrow and labelled. The image is divided in two parts, corresponding to two adjacent MOS slitlets, as the effect of the FORS2 polarization optics, which split the incoming light into two beams. The top and bottom parts of the image correspond to the extraordinary and ordinary beams, respectively, whereas the white stripe corresponds to the gap between the two adjacent MOS slitlets (see Section. 2.1 for details).

Finally, we used the RX J1856.5−3754 position in the master source list and the computed model PSF as input to the ALLSTAR routine in DAOPHOT to measure its flux through PSF photometry in each of the co-added 0°, 22°.5, 45°, *and* 67°.5 retarder-plate-angle images, and in both the ordinary and extraordinary beams. According to our experience with polarization measurements of such faint targets (see e.g. Mignani et al. 2015), PSF photometry is more robust than aperture photometry. In particular, we fitted the model PSF to the RX J1856.5−3754 intensity profile within an area of 10 pixel radius (2.5 arcsec), estimated from the growth curves of the reference stars and measured the sky background in an annulus of inner radius 10.5 pixels and width 10 pixels (2.6 and 2.5 arcsec), respectively. As a last step, we corrected the RX J1856.5−3754 flux for the atmospheric extinction using, for each image, the average of the measured airmass values and the extinction coefficients in the $v_{\rm HIGH}$ filter computed by the FORS2 quality control team.[4]

[4] www.eso.org/qc

We applied the same procedure as above to the polarized standard stars to calibrate the RX J1856.5−3754 polarization. From the comparison between the measured and reference values for the standard stars, we found that our polarimetry has, on average, an absolute uncertainty of only 0.13 ± 0.06 per cent in PD and of 0.°2 ± 0.°4 in PA. These values are consistent with both the trending analysis carried out by the FORS2 quality control team and with the independent analysis of Cikota et al. (2016), based upon six years of FORS2 observations of polarimetry standard stars. At the same time, from the observations of the unpolarized standard stars we found that there is no evidence of significant instrumental polarization (0.09 ± 0.06 per cent) at the CHIP1 aim position.

3 RESULTS

3.1 The RX J1856.5−3754 polarization

For the photometry parameters defined above, we measured a PD = 16.43 ± 5.26 per cent and a PA = 145.°39 ± 9.°44 for RX J1856.5−3754, where we computed the errors as described in Fossati et al. (2007). The target is faint, and hence the uncertainties are dominated by statistics rather than calibration.

With the measurement presented here, there are now six INSs for which the phase-averaged (or phase-resolved) linear polarization has been measured. Five of them are RPPs: the Crab and Vela pulsars, PSR B0540−69, PSR B1509−58, and PSR B0656+14 (see Mignani et al. 2015, and references therein), i.e. the five brightest RPPs identified in the optical (Mignani 2011). Therefore, RX J1856.5−3754 is the first INS other than an RPP for which a measurement of the optical polarization has been obtained. An upper limit on the optical linear polarization for the magnetar 4U 0142+61 (5.6 per cent at the 90 per cent c.l.) has been recently reported by Wang et al. (2015).[5]

We note that the polarization level measured for RX J1856.5−3754 seems to be above what measured for RPPs, for which the PD is usually below 10 per cent (see Mignani et al. 2015). The preferential orientation of the polarization vector is also different. Previous optical and/or radio polarization measurements in RPPs point towards a substantial alignment between the polarization vector and the proper motion direction (Mignani et al. 2015, and references therein). In the optical, this alignment has been measured for the Crab and Vela pulsars (Moran et al. 2013; Moran, Mignani & Shearer 2014) and, possibly, PSR B0656+14 (Mignani et al. 2015), whereas nothing can be said for both PSR B0540−69 and PSR B1509−58 for which no proper motion has been measured yet. In the case of RX J1856.5−3754, the polarization PA that we measured with the VLT (145.°39 ± 9.°44) and that of the proper motion (PA^{μ} = 100.°2 ± 0.°2; Kaplan et al. 2002) differ significantly (by ∼45°), even accounting for the substantial uncertainty of the former measurement, so the source does not appear to fit in this picture. It should be noted, however, that the emission process which produces the polarized optical radiation is different for RPPs and thermally emitting INSs, such as RX J1856.5−3754. In young RPPs, such as the Crab and Vela pulsars, the optical emission is produced in the neutron star magnetosphere (Pacini & Salvati 1983), i.e. along a preferred direction, whereas in thermally emitting INSs the optical radiation comes from the entire cooling neutron star surface.

[5] One measurement and two upper limits on the infrared polarization have been obtained for other three magnetars (Israel, private communication)

3.2 Remarks on the possibility of polarization contamination

RX J1856.5−3754 lies ∼1.°4 away from the centre of the dusty molecular cloud complex in the Corona Australis region (CrA). The distance to the CrA complex is, however, uncertain (see Neuhäuser & Forbrich 2008 for a discussion). Based upon measurements of the interstellar reddening from the *Hipparcos* and *Tycho* catalogues, Knude & Høg (1998) determined a distance of ∼170 pc. On the other hand, based upon the orbit solution of the eclipsing double-lined spectroscopic binary TY CrA (Casey et al. 1998), a distance as low as ∼130 pc was inferred. Therefore, we cannot firmly rule out either that the CrA dark cloud complex is foreground to RX J1856.5−3754 (123^{+11}_{-15} pc; Walter et al. 2010) or that this is embedded in it. In this case, although RX J1856.5−3754 is clearly away from the densest regions of the CrA complex, as seen from the Digitised Sky Survey images, it would still be possible that the more tenuous cloud limbs extend to the neutron star position. This might represent a possible source of contamination to our polarization measurement, which we would have to take into account. Indeed, stars embedded in, or in the background of, dust clouds are known to exhibit a non-zero degree of polarization, produced by starlight scattering on to the dust grains (e.g. Draine 2004, for a review). The observed degree of linear polarization $p(\lambda)$ usually follows the empirical Serkowski's law (Serkowski 1973):

$$p(\lambda) = p_{\max} \exp[-K \ln^2(\lambda/\lambda_{\max})], \quad (5)$$

where λ is the radiation wavelength; polarization attains a maximum, $p(\lambda) = p_{\max}$, at $\lambda = \lambda_{\max}$. In general K linearly depends on $\lambda_{\max}$ (e.g. Wilking, Lebofsky & Rieke 1982; Whittet et al. 1992; Cikota et al. 2016), while the maximum polarization $p_{\max}$ is found to be a function of the reddening (Serkowski 1973, and references therein), $p_{\max} \sim 0.09E(B-V)$. Since $\lambda_{\max} \sim 555$ nm (Serkowski, Mathewson & Ford 1975), which coincides with the pivot wavelength of the $v_{\rm HIGH}$ filter (Section. 2.1), the effects of dust on our measurement could be potentially relevant. The measured interstellar extinction towards RX J1856.5−3754 is $A_{\rm V} \sim 0.12$ (van Kerkwijk & Kulkarni 2001a), accounting for both gas and dust contributions, which gives $E(B-V) \sim 0.04$. Therefore, assuming that the CrA complex is, indeed, foreground to RX J1856.5−3754, the maximum degree of polarization predicted by the Serkowski's law in the $v_{\rm HIGH}$ filter ($\lambda \simeq \lambda_{\max}$) would be $p_{\max} \sim 0.36$ per cent.

The capacity of dust grains to produce polarization upon scattering depends on their degree of alignment, i.e. on how much their spin angular momenta point in the same direction (a still very debated issue; see e.g. Draine 2004). By adopting, as we did, $p_{\max} = 0.09E(B-V)$, some degree of alignment of the grains is already accounted for. However, it has been found that, along some directions, higher values of $p_{\max}$ are required to match the data with the Serkowski's law in the B and V bands (e.g. Clayton et al. 1992). This seems to imply a higher alignment of the grains along those lines of sight, which is associated with a reddening typically much larger than that observed along the line of sight (LOS) to RX J1856.5−3754. None the less, even assuming that a thin wisp of material with highly aligned grains lies in between us and RX J1856.5−3754 (e.g. connected with the bow-shock nebula associated with the source; van Kerkwijk & Kulkarni 2001b), it seems very unlikely that this could contribute to the observed PD by as much as 1 per cent.

This conclusion is confirmed by the values of the Stokes parameters $P_{\rm Q}$ and $P_{\rm U}$ measured for a set of 42 stars randomly selected within a region of a few arcmin size in the RX J1856.5−3754 field, as shown in Fig. 2. We selected stars in the magnitude range

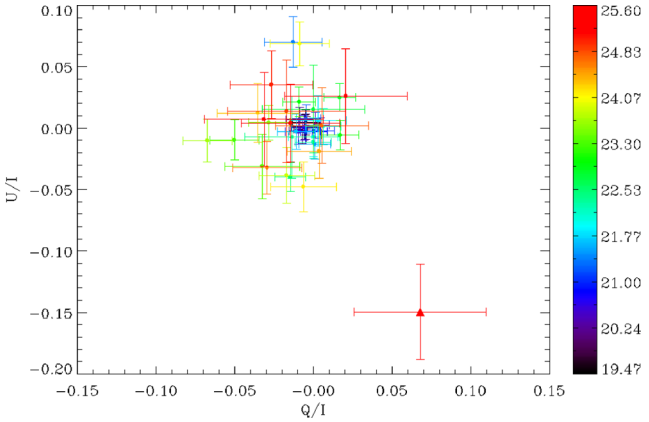

Figure 2. Plot of the normalized Stokes parameters U/I and Q/I for a selected sample of 42 field stars (filled point; top left) and for RX J1856.5−3754 (filled triangle, bottom right). We warn that the values of U/I and Q/I plotted here, computed from equations (1) and (2), are in unity fractions and so would be the value of PD computed from them (equation 3). The colour scale on the right corresponds to the stars' V-band magnitude.

∼20–26 and whose positions are more than 1 arcmin away from the CCD edges, to avoid the effects of off-axis instrumental polarization. We filtered out obvious outliers through a 3σ clipping and stars with errors larger than ∼5 per cent on the PD. Such stars are either saturated or with positions too close to the edges of the MOS slitlets, which affects the measurement of the fluxes f^{o} and f^{e}. We note that for the field stars the intrinsic degree of polarization is very small or even statistically compatible with zero; hence, the observed polarization would be essentially that produced by dust. On the other hand, for RX J1856.5−3754 the measured degree of polarization is substantial ($\gtrsim$11 per cent), ruling out that it could be due to dust. These arguments indicate that, in our case, dust contamination is also quite unimportant quantitatively.

Another possible source of polarization contamination could be the RX J1856.5−3754 bow-shock nebula itself. Indeed, free electrons in the shocked interstellar medium (ISM) may modify the polarization signal. However, the estimated number density ($\lesssim$3 cm^{-3}) in the shocked ISM surrounding RX J1856.5−3754 (van Kerkwijk & Kulkarni 2001b) is too small to make propagation effects such as scattering or Faraday conversion relevant in this context.

4 DISCUSSION

4.1 Comparison with theoretical models

The polarization properties of radiation emitted by the cooling surface of INSs are strongly influenced by QED vacuum polarization effects as photons propagate in the strongly magnetized vacuum that surrounds the star (e.g. Heyl & Shaviv 2000, 2002; Heyl et al. 2003; van Adelsberg & Lai 2006). A systematic analysis of the polarization properties (PD and PA) and of their dependence on the INS physical and geometrical parameters was presented by Taverna et al. (2015) in the case of pure BB surface emission. A specific application to the optical and X-ray polarization properties of RX J1856.5−3754 was recently discussed by González Caniulef et al. (2016), who also considered more realistic surface emission models, either a gaseous atmosphere (GA) or a condensed surface (CS), properly accounting for general-relativistic ray-bending and vacuum polarization effects. Their analysis assumed a dipolar magnetic field with an intensity at the pole $B_{\rm p} = 10^{13}$ G, as inferred from the spin-down measurements by van Kerkwijk & Kaplan (2008), and a dipole-induced surface temperature distribution with $T_{\rm p}^{\infty} = 60$ eV at the pole, truncated at $T_{\rm e}^{\infty} = 40$ eV at the equator, as it follows from the most recent spectral study of Sartore et al. (2012, see González Caniulef et al. 2016 for more details and Popov, Taverna & Turolla 2016 for a discussion of alternative thermal maps), where the temperatures are measured with respect to an observer at infinity. The star mass and radius were assumed to be $M_{\rm NS} = 1.5\,{\rm M}_{\odot}$ and $R_{\rm NS} = 12$ km, respectively, which imply a gravitational redshift factor at the surface $1 + z = 1.26$. In particular, González Caniulef et al. (2016) calculated the phase-averaged PD and PA as a function of the angles χ and ξ, which correspond to the inclination of the LOS and of the magnetic axis with respect to the INS spin axis, respectively, both in the soft X-rays (0.12–0.39 keV) and in the Cousins B filter ($\lambda = 445$ nm, $\Delta\lambda = 94$ nm).

Using the same approach described in González Caniulef et al. (2016), we computed the polarization properties in the $v_{\rm HIGH}$ band ($\lambda = 555.0$ nm, $\Delta\lambda = 61.6$ nm), in which our data were collected. We carried out the calculations for three different surface emission models: (i) an isotropic BB, assuming that the radiation is 100 per cent polarized in the extraordinary mode, (ii) a magnetized, completely ionized hydrogen atmosphere, and (iii) a CS model (both in the fixed and free ion limit; see again González Caniulef et al. 2016, for details). Results are summarized in Figs 3 and 4, which show the observed PD as a function of χ and ξ, and in Table 1. For the BB and the GA emission models, there is a range of angles that is consistent with the constraints set by the value of the X-ray pulsed fraction, (1.2 per cent; Tiengo & Mereghetti 2007), and the observed PD, 16.43 ± 5.26 per cent. In the first case, the angle between the LOS and the spin axis is $\chi = 15\overset{\circ}{.}6^{+1.8}_{-1.7}$ and the angle between the magnetic axis and the spin axis is $\xi = 18\overset{\circ}{.}0^{+2.4}_{-1.8}$, while in the second case it is $\chi = 14\overset{\circ}{.}0^{+2.3}_{-3.0}$ and $\xi = 3\overset{\circ}{.}1^{+0.8}_{-0.4}$. CS models provide a solution only in the fixed ion limit, $\chi = 21\overset{\circ}{.}7^{+5.9}_{-4.4}$ and $\xi = 5\overset{\circ}{.}5^{+1.4}_{-1.3}$, together with $\chi = 51\overset{\circ}{.}9^{+37.3}_{-14.7}$ and $\xi = 2\overset{\circ}{.}9^{+13.2}_{-0.4}$; the central value of the measured PD is never recovered in the free ion case. For all the considered emission models, our analysis points at small values of ξ, and $\chi \sim 15^{\circ}$–20° (in the case of CS emission model and the fixed ion limit there is a second solution at $\chi \sim 50^{\circ}$). This narrows the (broader) constraints set on the two geometrical angles by Ho (2007), $\chi \approx 20^{\circ}$–45° and $\xi \lesssim 6^{\circ}$ (or vice versa), on the basis of their pulse profile fits with atmospheric models. With the present estimate of the geometrical angles, a putative radio beam from RX J1856.5−3754 would not intersect the LOS, either assuming the pulsars average beaming factor, $f = 0.1$, or using the expression by Tauris & Manchester (1998) to relate f to the spin period (see also Ho 2007).

4.2 Test of QED predictions

Polarimetric observations offer a unique opportunity to experimentally verify the predictions of QED vacuum polarization effects in the strong-field limit. To test this, we recomputed the optical PD for RX J1856.5−3754 neglecting vacuum polarization effects. Results are shown in Figs 5 and 6. In all cases, the computed phase-averaged PD is substantially reduced, because the depolarization induced by the frame rotation is much more effective at small values of the adiabatic radius (with no QED vacuum polarization effects included the adiabatic radius coincides with the star radius; Heyl & Shaviv 2002; van Adelsberg & Lai 2006; Taverna et al. 2015; González Caniulef et al. 2016). The minimum attainable

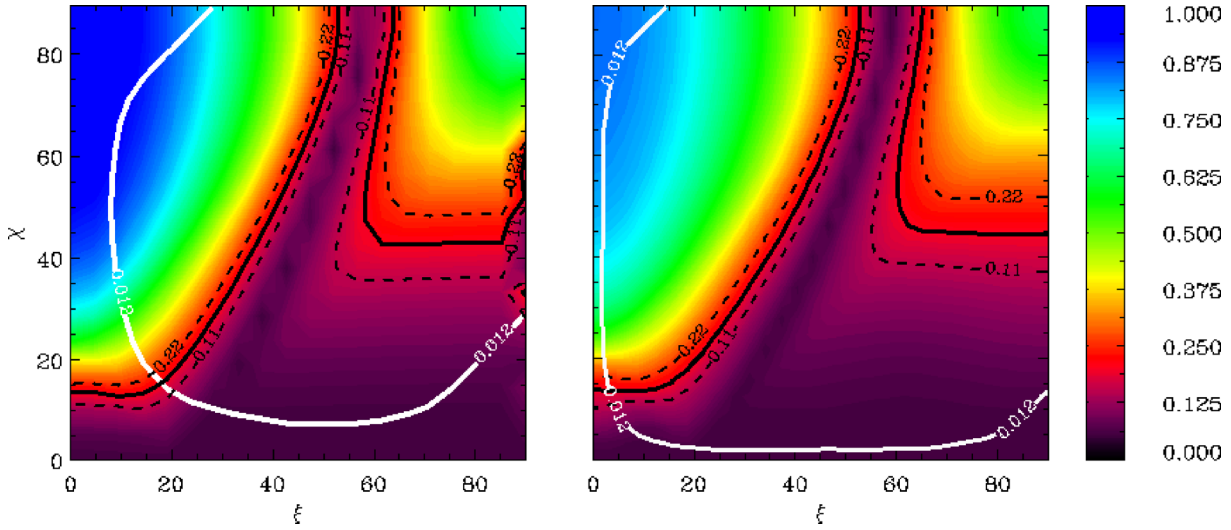

Figure 3. Contour plot of the phase-averaged linear PD in the VLT $v_{\rm HIGH}$ band for the isotropic blackbody (left) and the gaseous atmosphere (right) models. The thick white line marks the locus in the $\xi-\chi$ plane where the computed pulsed fraction matches the observed value, 1.2 per cent (Tiengo & Mereghetti 2007). The solid black line corresponds to the measured VLT optical polarization of RX J1856.5−3754 while the dashed lines correspond to the $\pm1\sigma$ error (PD = 16.43 ± 5.26 per cent).

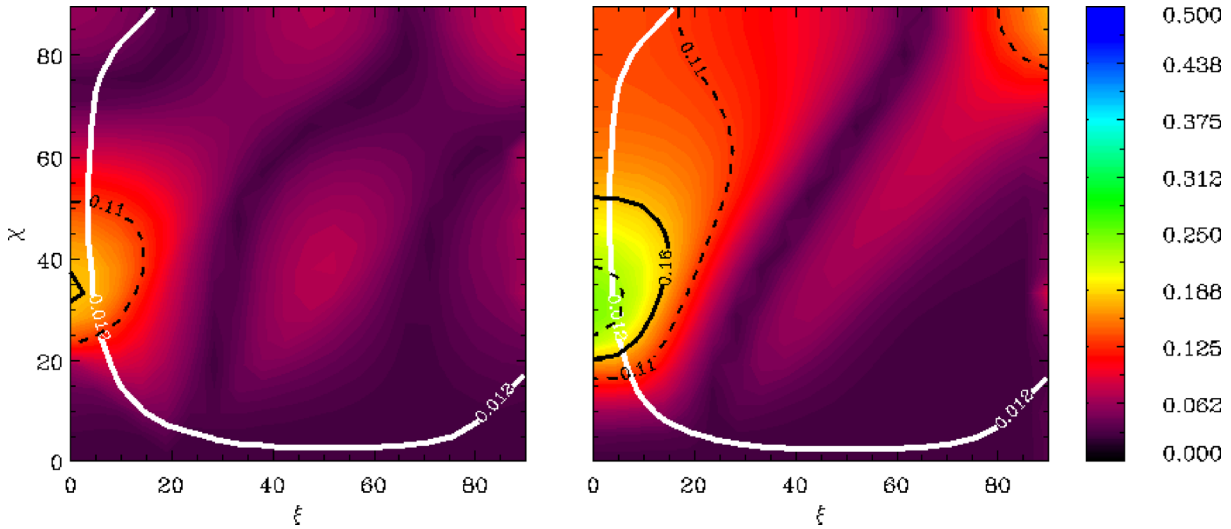

Figure 4. Same as in Fig. 3 for emission from a condensed surface in the free (left) and fixed ion limit (right).

Table 1. Summary of the values of χ and ξ obtained from the comparison of the measured PD and different emission models (first column).

Model	$\chi(^\circ)$	$\xi(^\circ)$
BB	$15.6^{+1.8}_{-1.7}$	$18.0^{+2.4}_{-1.8}$
GA	$14.0^{+2.3}_{-3.0}$	$3.1^{+0.8}_{-0.4}$
CS[a]	$21.7^{+5.9}_{-4.4}$	$5.5^{+1.4}_{-1.3}$
	$51.9^{+37.3}_{-14.7}$	$2.9^{+13.2}_{-0.4}$
Ho (2007)	≈ 20–45	$\lesssim 6$

Note. [a]Fixed ion limit.

phase-averaged PD is still within the measured range for the BB, GA, and CS (fixed ions) emission models, while it is not for the CS model in the free ion limit. However, the most likely measured value is never reproduced by models with no QED vacuum polarization effects, and the highest attainable PD, which is anyway below the measurement, requires a very particular geometry of the source, i.e. an aligned rotator ($\xi \approx 0^\circ$), seen equator-on ($\chi \approx 90^\circ$). The observed high value of the PD is therefore a strong indicator for the presence of vacuum polarization effects around RX J1856.5−3754.

4.3 Constraints on neutron star viewing orientations

The polarization PA provides independent information about the viewing orientations of the INS. We remark, however, that care must be taken in comparing the observed value with those derived from simulations since the PA depends on the choice of a reference direction in the plane of the sky. González Caniulef et al. (2016) computed the phase-averaged PA assuming as reference direction the projection of the star spin axis on the plane of the sky. In the case of the GA emission model, they found that the phase-averaged PA was nearly constant over almost the entire region where $\chi > \xi$ and assumes a value of ∼90°. This implies that, when 'phase-averaging' the signal, the direction of the electric field of the observed radiation

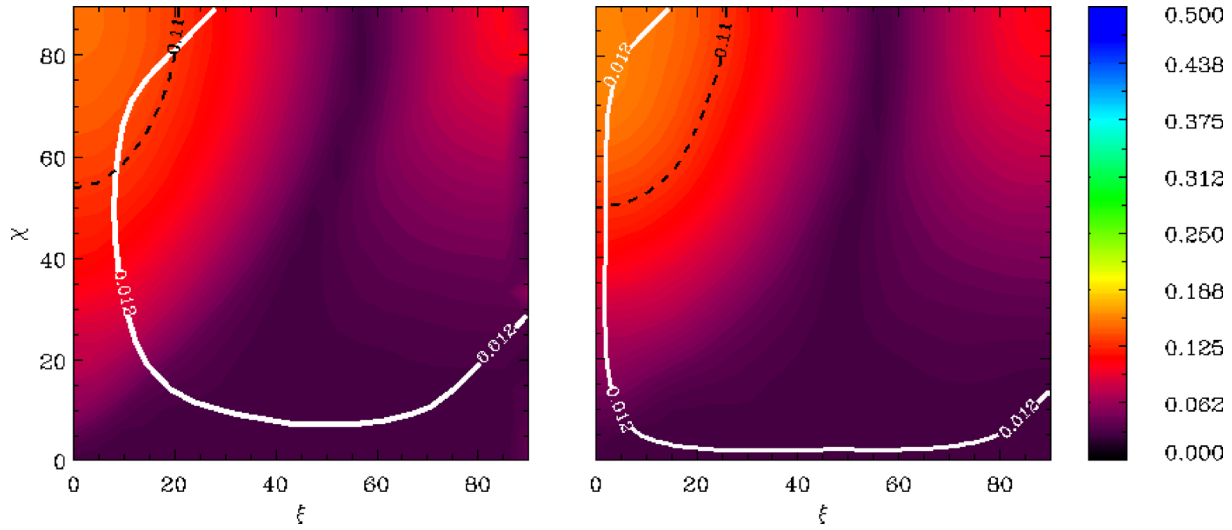

Figure 5. Same as in Fig. 3 but without accounting for vacuum polarization effects.

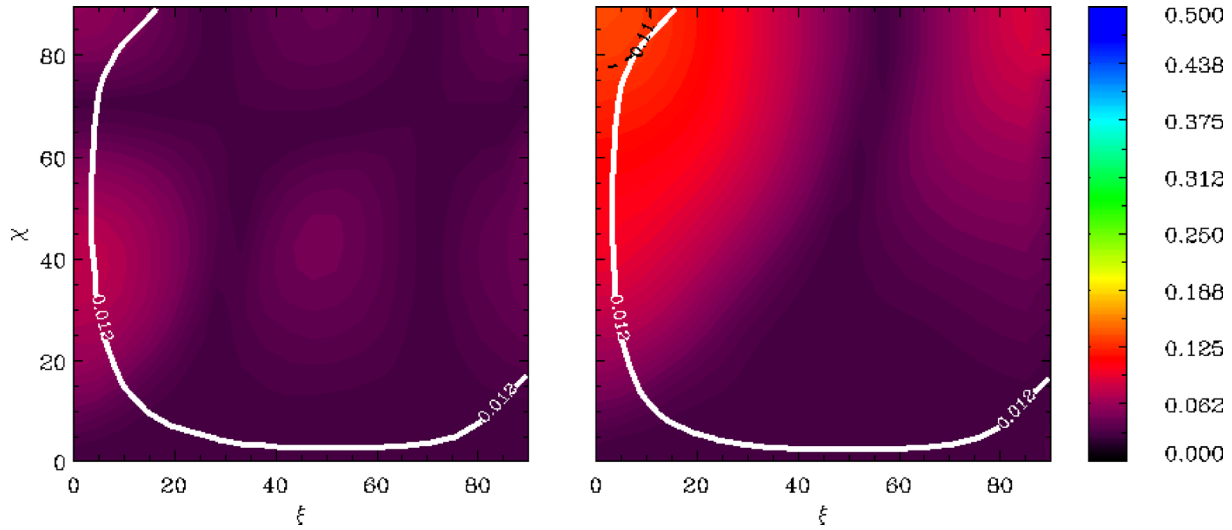

Figure 6. Same as in Fig. 4 but without accounting for vacuum polarization effects.

should oscillate mostly in a direction perpendicular to the star spin axis projected on the sky. For the CS emission model (here, we consider only the fixed ion limit since it matches the PD constraint), the situation is similar but somehow reversed, with PA $\sim 0^\circ$ in the region where $\chi > \xi$, meaning that the electric field oscillates mainly along the projection of the spin axis.

Our VLT polarimetry observations of RX J1856.5−3754 give a polarization PA $= 145\overset{\circ}{.}39 \pm 9\overset{\circ}{.}44$, where this angle is computed using as reference direction the North Celestial Meridian. As for the PD, we recomputed the PA in the VLT $v_{\rm HIGH}$ band, obtaining results very similar to those of González Caniulef et al. (2016), i.e. PA $= 90^\circ$ and 0° for the GA and the CS models, respectively. As discussed above, we need to introduce a rotation by an angle β around the LOS, to account for the different reference direction in the simulations and in the observations.[6] In this case, β obviously corresponds to angle between the projection of the neutron star spin axis on the plane of the sky and the North Celestial Meridian. Therefore, we can obtain for the first time the absolute direction of the spin axis of RX J1856.5−3754 in the plane of the sky. We found that, for the atmosphere model, a rotation angle $\beta = 55\overset{\circ}{.}39 \pm 9\overset{\circ}{.}44$ (or $235\overset{\circ}{.}39 \pm 9\overset{\circ}{.}44$) reproduces the observed value, for the viewing angles derived in Section 4.1 ($\chi = 14\overset{\circ}{.}0^{+2.3}_{-3.0}, \xi = 3\overset{\circ}{.}1^{+0.8}_{-0.4}$). Similarly, a rotation angle $\beta = 145\overset{\circ}{.}39 \pm 9\overset{\circ}{.}44$ (or $325\overset{\circ}{.}39 \pm 9\overset{\circ}{.}44$) is required for the CS model (fixed ions); see Fig. 7.

From the value of β, we can derive the angle θ between the projection of the neutron star spin axis on the plane of the sky and the neutron star proper motion vector, where $\theta = {\rm PA}^\mu - \beta$ and ${\rm PA}^\mu = 100\overset{\circ}{.}2 \pm 0\overset{\circ}{.}2$ (Kaplan et al. 2002). For the atmospheric case ($\beta = 55\overset{\circ}{.}39 \pm 9\overset{\circ}{.}44$), we obtain that the direction of the spin axis of RX J1856.5−3754 is tilted westwards of the neutron star proper motion vector by an angle $\theta = 44\overset{\circ}{.}81 \pm 9\overset{\circ}{.}64$. In the case of the CS emission model ($\beta = 145\overset{\circ}{.}39 \pm 9\overset{\circ}{.}44$), instead, we obtain that the projection of the spin axis is tilted eastwards of the proper motion vector by $\theta = 45\overset{\circ}{.}19 \pm 9\overset{\circ}{.}64$. Therefore, in both cases the projection of the spin axis and the proper motion vector are significantly misaligned.

[6] This amounts to a rotation of the Stokes parameters by an angle 2β around the LOS, which clearly leaves the PD unchanged.

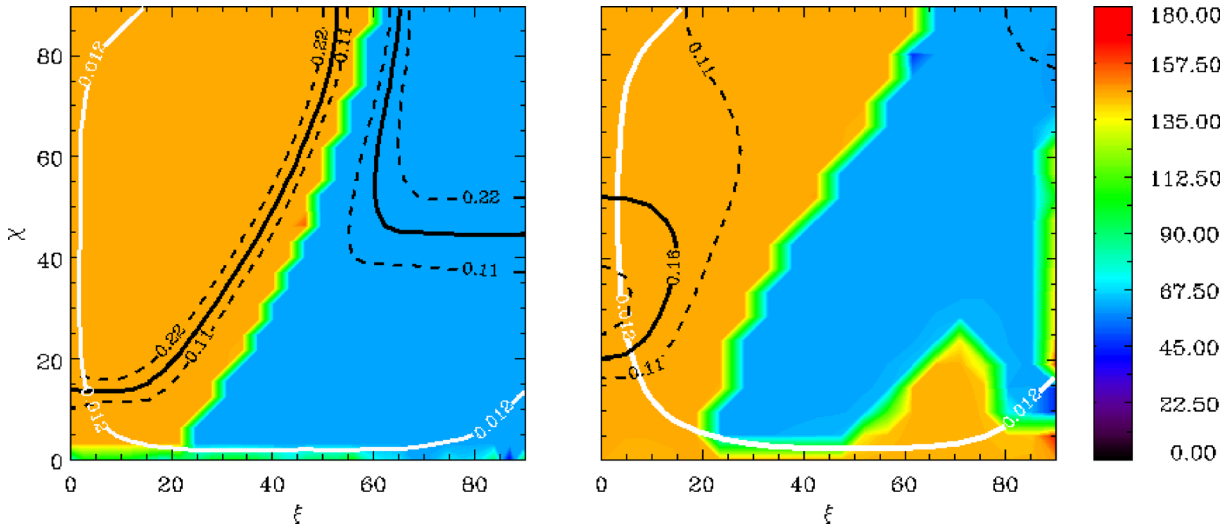

Figure 7. Contour plot of the phase-averaged linear polarization PA in the VLT $\nu_{\rm HIGH}$ band for emission from a gaseous atmosphere (left) and a condensed surface (fixed ion limit; right). In each case a rotation by an angle β around the LOS has been applied (see Section 4.3 for details). The labelled contours have the same meaning as in Fig. 3.

Although this is still a debated issue, it has been suggested that in the Crab and Vela pulsars the direction of the spin axis projected in the plane of the sky, assumed to coincide with the axis of symmetry of their X-ray pulsar wind nebulae (PWNe), coincides with that of the proper motion (Helfand, Gotthelf & Halpern 2001; Pavlov et al. 2001, see also Kaplan et al. 2008). Noutsos et al. (2012) presented a statistical analysis based on a large sample of pulsars with proper motion and polarization measurement, and found evidence for pulsar spin-velocity alignment, although the possibility of orthogonal spin-velocity configurations could not be excluded. Such an alignment derives from that of the pulsar rotation axis and the velocity vector. The latter can be produced if the protoneutron star kick resulted from multiple thrusts over a time longer than the star initial period. On the other hand, no correlation is expected if the acceleration phase is shorter (Spruit & Phinney 1998). Therefore, the ∼45° misalignment that we found in RX J1856.5−3754 might not be peculiar, also accounting for the fact that the velocity vector might have changed over the source lifetime, ∼0.42 Myr, as the result of the interaction with the Galactic gravitational potential (e.g. Mignani et al. 2013). For comparison, in the case of the radio-quiet RPP Geminga, of age (≈0.3 Myr) comparable to RX J1856.5−3754, the pulsar spin axis (again assumed to coincide with the axis of symmetry of its PWN) and the proper motion vector are aligned (Pavlov, Bhattacharyya & Zavlin 2010). This would suggest that their relative orientation has not been affected by the pulsar orbit in the Galactic potential (Pellizza et al. 2005).

5 SUMMARY AND CONCLUSIONS

We presented the first measurement of optical polarization from a thermally emitting INS, RX J1856.5−3754. We measured a linear PD = 16.43 ± 5.26 per cent and a polarization PA = 145.°39 ± 9.°44. At variance with the case of RPPs, in which polarization measurements give an indication of the magnetic field direction in the magnetosphere (Mignani et al. 2015 and references therein), in the case at hand the polarization observables are directly linked to the properties of the surface (or atmospheric) layers of the neutron star. As already pointed out by González Caniulef et al. (2016), optical measurements complemented by measurements of X–ray polarization can be used to discriminate between the case of a gaseous atmosphere and a condensed neutron star surface layer for different viewing geometries. Thus, our measurement paves the way to future X-ray polarimetry measurements in the soft X rays (e.g. Marshall et al. 2015). In any case, we found that, independently on how thermal photons are produced, such a high value of linear polarization in the signal is extremely unlikely to be reproduced by models in which QED vacuum polarization effects are not accounted for. Therefore, our VLT polarization measurement constitutes the very first observational support for the predictions of QED vacuum polarization effects. Follow-up optical polarimetry observations of RX J1856.5−3754 will confirm and improve our measurement and make the observational support to the QED predictions more robust. Optical-polarimetry measurements of some of the other M7 would be obviously important to consolidate our results, although such measurements would be more challenging owing to the fact that the other M7 are even fainter than RX J1856.5−3754 (Kaplan et al. 2011). Imaging polarimetry capabilities at the next generation of 30–40m class telescopes, such as the European Extremely Large Telescope, would then play a crucial role in testing QED predictions of vacuum polarization effects on a larger sample. Measurements of the circular optical polarization, never obtained so far for any INS other than the Crab pulsar (Wiktorowicz et al. 2015), should also be pursued. Circular polarization for thermal radiation coming from the neutron surface is zero in the approximation adopted in this work (a sharp boundary for the adiabatic region; see Taverna et al. 2015) and, according to our numerical simulations, it is expected not to exceed 1–2 per cent even accounting for the presence of an intermediate region, the only place where circular polarization can be created (Taverna et al. 2014, 2015). The measurement of such a small PD could be attainable, again, only exploiting the high throughput of the next generation of extra-large telescopes.

ACKNOWLEDGEMENTS

This work is based on the observations collected at the European Organisation for Astronomical Research in the Southern Hemisphere under ESO programme 095.D-0343(A). We thank the anonymous referee for his/her very constructive comments to

our manuscript. RPM acknowledges financial support from the project TElescopi CHErenkov made in Italy (TECHE).it. CRA 1.05.06.04.01 cap 1.05.08 for the project 'Studio multi-lunghezze d'onda da stelle di neutroni con particolare riguardo alla emissione di altissima energia'. DGC acknowledges the financial support by CONICYT through a 'Becas Chile' fellowship no. 72150555.

REFERENCES

Appenzeller I. et al., 1998, Messenger, 94, 1
Boffin H. M. J., 2014, The FORS2 User Manual. European Southern Observatory, Garching, Germany
Casey B. W., Mathieu R. D., Vaz L. P. R., Andersen J., Suntzeff N. B., 1998, AJ, 115, 1617
Cikota A., Patat F., Cikota S., Faran T., 2016, MNRAS, preprint (arXiv:1610.00722)
Clayton G. C. et al., 1992, ApJ, 385, L53
Draine B. T., 2004, in Pfnenniger D., Revaz Y., eds, Saas-Fee Advanced Course Vol. 32. The Cold Universe. Springer-Verlag, Berlin, p. 231
Fossati L., Bagnulo S., Mason E., Landi Degl'Innocenti E., 2007, in Sterken C., ed., ASP Conf. Ser. Vol. 364, The Future of Photometric, Spectroscopic, and Polarimetric Standardization. Astron. Soc. Pac., San Francisco, p. 503
González Caniulef D., Zane S., Taverna R., Turolla R., Wu K., 2016, MNRAS, 459, 3585
Heisenberg W., Euler H., 1936, Z. Phys., 98, 714
Helfand D. J., Gotthelf E. V., Halpern J. P., 2001, ApJ, 556, 380
Heyl J. S., Shaviv N. J., 2000, MNRAS, 311, 555
Heyl J. S., Shaviv N. J., 2002, Phys. Rev. D, 66, 023002
Heyl J. S., Shaviv N. J., Lloyd D., 2003, MNRAS, 342, 134
Ho W. C. G., 2007, MNRAS, 380, 71
Kaplan D. L., van Kerkwijk M. H., Anderson J., 2002, ApJ, 571, 447
Kaplan D. L., Chatterjee S., Gaensler B. M., Anderson J., 2008, ApJ, 677, 1201
Kaplan D. L., Kamble A., van Kerkwijk M. H., Ho W. C. G., 2011, ApJ, 736, 117
Knude J., Høg E., 1998, A&A, 338, 897
Lasker B. M. et al., 2008, AJ, 136, 735
Marshall H. L., Schulz N. S., Windt D. L., Gullikson E. M., Craft M., Blake E., Ross C., 2015, in O'Dell S. L., Pareschi G., eds, Proc. SPIE Conf. Ser. Vol. 9603, Optics for EUV, X-Ray, and Gamma-Ray Astronomy VII. SPIE, Bellingham, p. 960319
Mathewson D. S., Ford V. L., 1971, MNRAS, 153, 525
Mignani R. P., 2011, Adv. Space Res., 47, 1281
Mignani R. P. et al., 2013, MNRAS, 429, 3517
Mignani R. P., Moran P., Shearer A., Testa V., Słowikowska A., Rudak B., Krzeszowski K., Kanbach G., 2015, MNRAS, 583, 105
Moran P., Shearer A., Mignani R. P., Słowikowska A., De Luca A., Gouiffes C., Laurent P., 2013, MNRAS, 433, 2564
Moran P., Mignani R. P., Shearer A., 2014, MNRAS, 445, 835
Neuhäuser R., Forbrich J., 2008, in Reipurth B., ed., ASP Monogr. Publ. Vol. 5, Handbook of Star Forming Regions: Volume II, The Southern Sky. Astron. Soc. Pac., San Francisco, p. 735
Noutsos A., Kramer M., Carr P., Johnston S., 2012, MNRAS, 423, 2736
Pacini F., Salvati M., 1983, ApJ, 274, 369
Pavlov G. G., Kargaltsev O. Y., Sanwal D., Garmire G. P., 2001, ApJ 554, L189
Pavlov G. G., Bhattacharyya S., Zavlin V. E., 2010, ApJ, 715, 66
Pellizza L. J., Mignani R. P., Grenier I. A., Mirabel I. F., 2005, A&A, 435, 625
Popov S. B., Taverna R., Turolla R., 2016, MNRAS, preprint (arXiv:1610.05050)
Potekhin A. Y., 2014, Phys.-Usp., 57, 735
Sartore N., Tiengo A., Mereghetti S., De Luca A., Turolla R., Haberl F., 2012, A&A, 541, 66
Serkowski K., 1973, in Greenberg J. M., van de Hulst H. C., eds, Proc. IAU Symp. 52, Interstellar Dust and Related Topics. Reidel, Dordrecht, p. 145
Serkowski K., Mathewson D. S., Ford W. L., 1975, ApJ, 196 261
Soffitta P. et al., 2013, Exp. Astron., 36, 523
Spruit H., Phinney E. S., 1998, Nature, 393, 139
Stetson P. B., 1987, PASP, 99, 191
Stetson P. B., 1994, PASP, 106, 250
Tauris T. M., Manchester R. N., 1998, MNRAS, 298, 62
Taverna R., Muleri F., Turolla R., Soffitta P., Fabiani S., Nobili L., 2014, MNRAS, 438, 1686
Taverna R., Turolla R., Gonzalez Caniulef D., Zane S., 2015, MNRAS, 454, 3254
Tiengo A., Mereghetti S., 2007, ApJ, 657, L101
Turolla R., 2009, in Becker W., ed., Astrophysics and Space Science Library Vol. 357, Neutron Stars and Pulsars. Springer, Berlin, p. 141
Turolla R., Zane S., Drake J. J., 2004, ApJ, 603, 265
van Adelsberg M., Lai D., 2006, MNRAS, 373, 1495
van Kerkwijk M. H., Kaplan D. L., 2008, ApJ, 673, L163
van Kerkwijk M. H., Kulkarni S. R., 2001a, A&A, 378, 986
van Kerkwijk M. H., Kulkarni S. R., 2001b, A&A, 380, 221
Walter F. M., Matthews L. D., 1997, Nature, 389, 358
Walter F. M., Eisenbeiss T., Lattimer J. M., Kim B., Hambaryan V., Neuhäuser R., 2010, ApJ, 724, 669
Wang Z., Tanaka Y. T., Wang C., Kawabata K. S., Fukazawa Y., Itoh R., Tziamtzis A., 2015, ApJ, 814, 89
Weisskopf V., 1936, Mat.-Fys. Medd. K. Dan. Vidensk. Selsk. 14, 1
Weisskopf M. C. et al., 2013, in Siegmund O. H., ed., Proc. SPIE Conf. Ser. Vol. 8859, UV, X-Ray, and Gamma-Ray Space Instrumentation for Astronomy XVIII. SPIE, Bellingham, p. 885908
Whittet D. C. B., Martin P. G., Hough J. H., Rouse M. F., Bailey J. A., Axon D. J., 1992, ApJ, 386, 562
Wiktorowicz S., Ramirez-Ruiz E., Illing R. M. E., Nofi L., 2015, Am. Astron. Soc. Meeting, 225, 421.01
Wilking B. A., Lebofsky M. J., Rieke G. H., 1982, AJ, 87, 695

This paper has been typeset from a TEX/LATEX file prepared by the author.